

# AIGOR: A Modular, Event-Driven Neuromorphic Architecture for Configurable SNN Inference

Pierpaolo Perticaroli<sup>\*1</sup>, Roberto Ammendola<sup>2</sup>, Andrea Biagioni<sup>1</sup>, Ottorino Frezza<sup>1</sup>, Francesca Lo Cicero<sup>1</sup>, Michele Martinelli<sup>1</sup>, Pier Stanislao Paolucci<sup>1</sup>, Elena Pastorelli<sup>1</sup>, Luca Pontisso<sup>1</sup>, Cristian Rossi<sup>3,1</sup>, Francesco Simula<sup>1</sup>, Piero Vicini<sup>1</sup>, and Alessandro Lonardo<sup>1</sup>

<sup>1</sup>Istituto Nazionale di Fisica Nucleare, Sezione di Roma, Rome, Italy

<sup>2</sup>Istituto Nazionale di Fisica Nucleare, Sezione di Roma Tor Vergata, Rome, Italy

<sup>3</sup>Università Sapienza di Roma, Rome, Italy

July 7, 2026

## Abstract

Spiking neural networks (SNNs) run today on a fragmented landscape of hardware: dedicated neuromorphic processors, application-specific FPGA accelerators, and large-scale neuroscience simulators, each typically built around a fixed neuron model, execution strategy, or workload class. We present AIGOR, a modular, event-driven neuromorphic architecture for spiking neural network inference. AIGOR organizes neurons into timestep-synchronized processing cores that exchange spikes as packets over a packet-switched communication layer, and it is assembled from a library of parameterized compute, memory, and communication IP blocks rather than as a one-off design for a single network. The neuron model, numeric precision, the folding of neurons onto hardware, and the partitioning across cores are configured per instance rather than committed at design time; a single declarative specification then generates the cores, neuron kernels, and synaptic-memory images that realize a given network.

We validate a first prototype on the AMD Versal VPK180 across two deliberately different workloads mapped onto the same cores: a feedforward image classifier trained in `snnTorch` and a recurrent balanced random network modeled in `NEST`. The classifier reproduces its `snnTorch` reference accuracy, and the recurrent network matches its `NEST` reference at spike-level precision across multiple cores spanning two FPGAs. We report post-implementation resource utilization

---

\*Corresponding authors: [pierpaolo.perticaroli@roma1.infn.it](mailto:pierpaolo.perticaroli@roma1.infn.it), [alessandro.lonardo@roma1.infn.it](mailto:alessandro.lonardo@roma1.infn.it)

and validate the multi-node synchronization scheme in simulation up to one thousand cores on a three-dimensional torus. The prototype’s measured limits localize the throughput bottleneck in the synaptic-delivery datapath and the global timestep barrier, and motivate a set of datapath refinements, now in development, that the configurable structure of the architecture admits as changes to the same cores.

## 1 Introduction

Spiking neural networks are studied and deployed across communities with rather different goals and tools. In machine learning, SNNs are pursued as an energy-efficient, event-driven alternative to conventional deep networks [14, 23] and are trained with surrogate-gradient methods [24, 10], often run on dedicated neuromorphic processors [18, 19] or on application-specific accelerators. In computational neuroscience, large recurrent networks are simulated to study brain dynamics [13] on CPU/GPU clusters or on specialized simulation engines [11, 12]. A related strand pursues SNNs for real-time inference at the data source in high-energy-physics experiments [25, 26]. Alongside these sits a broad body of FPGA implementations spanning both worlds. The result is a fragmented landscape with little common ground across neuron models, execution strategies, and workload classes.

Many application-specific designs commit a neuron model, a numeric precision, a degree of parallelism, an interconnect, and a connectivity pattern at design time, tailoring the compute logic, the software-ingestion path, and the communication to a single use case. Such designs are effective for their target workload but are not easily retargeted to a different network class. Rigidity is addressed in two established ways: large programmable platforms such as SpiNNaker and Loihi run a broad range of models on fixed hardware [21, 16, 17], while a growing body of FPGA frameworks generates a configured accelerator from a high-level description [28, 29]. AIGOR follows the latter direction, resolving the neuron model, numeric format, parallelism, and partitioning when an instance is generated, so that one description can produce hardware for different network classes.

AIGOR organizes neurons into processing cores that all advance the same discrete timestep together, exchanging spikes as packets over a packet-switched communication layer; input/output cores form the boundary with the outside world. The architecture is built from modular compute, memory, and communication components, and a single declarative specification drives a generation flow that emits a complete synthesizable instance together with the synaptic-memory images that map a given network onto it. The operating point of an instance, summarized by the configuration axes in Table 1, is a property of the specification rather than a design-time commitment. The current prototype is realized on up to two Versal VPK180 FPGAs, where the same architecture scales from a single device to a multi-node deployment,

with larger topologies exercised in simulation.

This paper describes the architecture, the generation flow that produces instances of it, and a methodology for validating and characterizing those instances, and it exercises the architecture on two deliberately different SNN workload classes. Concretely, it makes the following contributions:

- **A modular, event-driven neuromorphic architecture.** AIGOR defines a timestep-synchronized execution model in which a library of parameterized compute, memory, and communication blocks composes into processing cores. Configurable workers host and update the neurons, accumulating each neuron’s incoming synaptic contributions per receptor and per delay slot in circular delay buffers before the neuron is evaluated, and spikes travel between cores as packets over a packet-switched network (Section 3).
- **Configuration as an architectural property.** The neuron model, numeric precision, the spatial-versus-temporal folding of neurons onto hardware, and the partitioning of neurons across cores and workers are exposed as parameters of the IP blocks rather than fixed design decisions. A single declarative YAML specification expands together into the core RTL, the neuron kernels, and the initialized synaptic-memory images of a synthesizable instance (Section 4).
- **One system across SNN regimes.** We map and run two workloads usually addressed by separate systems, a feedforward image classifier trained in `snnTorch` and a recurrent balanced random network (Brunel-style) modeled in NEST, onto the same cores, differing only in their generated configuration. The classifier reproduces its `snnTorch` reference accuracy; the recurrent benchmark is validated at spike-level precision against its NEST reference across multiple cores spanning two FPGAs (Section 6).
- **A prototype, its characterization, and a roadmap.** We report functional validation and post-implementation resource utilization for a Versal VPK180-based prototype, and validate the multi-node synchronization scheme in simulation up to one thousand cores. From the prototype’s measured limits we derive a set of datapath refinements, a banked synaptic accumulator, a fused single-word spike/sync protocol, and globally-asynchronous locally-synchronous timestep synchronization, presented as the next stage of the architecture (Section 7).

AIGOR’s parameterized structure means a broad range of hardware instances can be derived from one description, providing a natural basis for the systematic exploration of SNN hardware design trade-offs. The objective of this paper is to present the architecture and the flow that instantiates it,

to describe a prototype on Versal FPGAs, and to validate it across distinct classes of spiking-neural-network workloads.

## 2 Background and Related Work

**Spiking neural networks and their hardware.** SNNs communicate through sparse, asynchronous spike events and carry state (membrane potential together with synaptic and adaptation variables) that evolves in discretized time [8, 9]. They are realized across a wide range of hardware, from mixed-signal [20] and digital neuromorphic ASICs to FPGA accelerators and large-scale simulation engines [14, 15]. These systems differ mainly in how much they fix in advance: application-specific accelerators commit the neuron model, numeric precision, connectivity, and synaptic-delivery scheme up front and optimize the result for one workload class, which is efficient for that workload but hard to retarget.

**Programmable neuromorphic platforms.** A complementary approach keeps the hardware fixed and obtains breadth through programmability. SpiNNaker realizes neuron and synapse dynamics in software on a packet-switched array of general-purpose cores, relaxing memory coherence, synchrony, and determinism so that arbitrary models can run on the same machine [21]; its second generation keeps this software-defined approach while adding numerical accelerators and scaling to far more cores [22]. Intel’s Loihi and Loihi 2 keep the silicon fixed while exposing programmable neuron models, graded spikes, and on-chip learning over an asynchronous mesh [16, 17]. These designs show that a neuromorphic architecture can be valued for the range of models and workloads it supports rather than for a single efficiency figure. AIGOR shares this orientation but reaches it differently: the model, precision, datapath, and parallelism are resolved when an instance is generated and synthesized, so each configuration is a tailored hardware build rather than a program running on fixed silicon.

**FPGA SNN systems.** On FPGAs, two tendencies are visible. One targets a specific workload at scale: NeuroAix, for example, is an FPGA cluster for accelerated, deterministic neuroscience simulation, built around leaky integrate-and-fire neurons with current-based synapses for the cortical-microcircuit benchmark [27]. The other generates a configured accelerator from a high-level description, as in Spiker+, which produces compact multi-layer SNN accelerators for edge inference [28]; recent work continues in this direction, adding configurable precision and topology or multi-FPGA scaling [29, 30, 31]. AIGOR belongs to this second group and differs in the range of choices it draws from one specification: neuron model, numeric precision, spatial-temporal folding, and partitioning across cores. Where these systems

usually hold one of these fixed, a neuron model or a workload class, AIGOR leaves them open and exercises both a feedforward classifier and a recurrent network on the same cores.

**Composition and transport.** AIGOR builds its inter-core communication on the APEIRON framework [2], a low-latency, packet-switched fabric developed for distributed real-time inference in high-energy-physics data acquisition, a domain with a long line of FPGA-based front-end and inference systems [6, 3, 4, 5]. This lineage orients AIGOR toward streaming inference at the data source, a setting we pursue for the ePIC dual-radiator RICH detector [7] in a companion study [32], and provides the multi-node transport over which a partitioned network spans several FPGAs.

### 3 AIGOR Architecture

This section describes the AIGOR architecture as realized in the current prototype; the generation flow that produces a concrete instance is described in Section 4. The structural choices below, the neuron model, the numeric format, the datapath width, the degree of parallelism, and the partitioning of neurons across cores and workers, are set when an instance is generated rather than fixed once for all instances; together they form the configuration axes of Table 1. All instances share the same interfaces, the same timestep-synchronized execution, and the same routing fabric, so that a given instance is one point in this space.

Table 1: Principal AIGOR configuration axes exposed to design-space exploration in the current prototype. Additional axes introduced by the refinements of Section 7 (synaptic-delivery scheme and inter-core routing policy) extend this space.

Axis	Variants / range	Trade-off governed
Numeric format	float / fixed-point (tunable widths)	accuracy vs. area/timing
Neuron model	LIF / IAF / adaptive-exp. / ...	expressivity vs. cost
Neuron compute	spatial / time-multiplexed	latency vs. area
Cores per system	$\geq 1$ (multi-FPGA)	capacity / partitioning
Workers per core	$\geq 1$	intra-core parallelism
Neurons per worker	$\geq 1$	spatial-temporal folding

#### 3.1 System organization

An AIGOR system is a set of *cores* interconnected by a routing fabric (Fig. 1). *SNN cores* host the neurons and run their dynamics; *I/O cores*

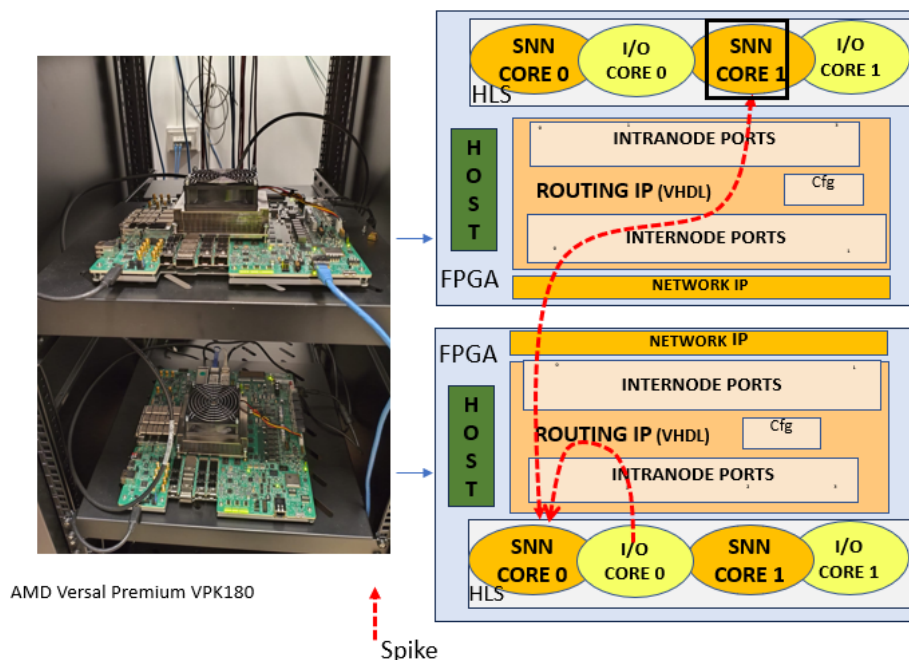


Figure 1: AIGOR prototype deployed across two AMD Versal Premium VPK180 boards. *Left:* the two-board setup. *Right:* the per-FPGA organization. On each device the SNN cores and I/O cores are synthesized as HLS kernels and attach to the APEIRON routing IP (VHDL), which exposes *intra-node* ports for on-chip core-to-core traffic and *inter-node* ports that reach the network IP driving the physical inter-FPGA link; a configuration block (Cfg) holds the routing tables, and the host (the board’s Arm APU) injects stimulus and reads results through the I/O cores. The red dashed path traces a single spike: originating on the lower FPGA, it is switched by the routing IP and, because its postsynaptic target resides on the other device, leaves through the inter-node ports and network IP, crosses to the upper FPGA, and is delivered by that FPGA’s routing IP to the destination SNN core (highlighted). Delivery is transparent to the cores: the same packet interface carries a spike whether its target sits on the same device or across the torus.

form the boundary with the outside world, encoding external data (detector frames, event-camera streams, or externally generated Poisson sources) into spikes and collecting results. In the current prototype a *host*, the Versal board’s Arm-based Application Processing Unit (APU), injects stimulus and reads outputs through the I/O cores, and reads and writes status and configuration registers. Cores occupy positions on a logical three-dimensional torus of nodes, so that a single specification scales from one device to a multi-FPGA partition without changing the core design.

Inter-core transport is provided by the APEIRON framework (Section 2), which supplies a packet-switched, low-latency communication IP, the *routing IP*, that carries events between cores intra-node and inter-node across the torus. Each AIGOR core attaches to this routing IP and exchanges spikes as packets. Because computation and transport are decoupled, the cores are composable: the routing IP is the same fabric in every configuration.

Execution combines *event-driven* communication with global *timestep synchronization*. Communication and synaptic gathering are event-driven: only the spikes actually emitted in a timestep trigger synaptic-memory fanout reads and accumulation, so a core does no synaptic work for silent inputs. Neuron updates, by contrast, are timestep-driven: every neuron’s state is advanced once per timestep, so the model is discrete-time. Within a timestep, the spikes emitted in the previous step are delivered, accumulated, and integrated; the step then closes with a synchronization (*sync*) event that advances each core’s timestep counter and keeps all cores globally synchronized, ensuring no spike is misordered or lost. Every event a core exchanges carries a leading sync bit: a spike event carries the presynaptic identifier in the manner of an address-event representation [1], while a sync event carries only the originating core and the timestep, signaling the barrier. In the prototype the barrier is a dedicated per-core sync packet, exchanged once per timestep. Sample boundaries, when required for inference, are handled either by an end-of-sample marker or by a fixed timestep window driven from a configuration register, at which point the neuron states are reset.

### 3.2 The SNN core

A network is partitioned hierarchically by the *AIGOR loader*, a software toolchain that groups neurons into workers, workers into cores, and cores across FPGAs, and emits the per-core synaptic-memory images that encode the mapped connectivity. Two configurable choices determine how a core realizes its neurons: how each worker computes its neurons, and how synaptic input reaches them.

The first choice is how a worker computes its neurons. In the *spatial* (worker-parallel) organization a worker holds one physical datapath per neuron and updates them concurrently, maximizing parallelism and minimizing latency; in the *time-multiplexed* organization a single datapath is folded over

the worker’s neurons, exchanging cycles for area and making large populations tractable on a fixed silicon budget. Combined with the partitioning knobs (number of cores, workers per core, and neurons per worker) this places the same network anywhere from maximally parallel to maximally folded.

The second choice is how synaptic input is delivered. The prototype uses *local per-worker routing* (Fig. 2), in which accumulation happens inside the workers rather than in a shared block. An incoming spike indexes a *synaptic memory*, held in on-chip URAM on the VPK180, that stores per presynaptic source the fanout of target connections. A *memory handler* streams the addressed fanout and unpacks each connection into a synapse word carrying its weight, synaptic delay, and receptor identifier, marking the last word of the timestep’s traffic so downstream stages know when the barrier has been reached. Each synapse word is then routed to the worker that hosts its destination neuron, where the destination identifier  $ID_{\text{post}}$  is resolved into a local (neuron, receptor) pair. Routed words are buffered in per-receptor input FIFOs and merged by a round-robin stage into each worker’s accumulation path. There, each contribution lands in a circular delay buffer held per (neuron, receptor): a `MAX_DELAY`-slot ring indexed by the synaptic delay relative to a head pointer that rotates once per timestep, so that a delayed contribution surfaces in the correct future timestep. At the timestep boundary each buffer’s head slot is read into the worker’s neuron-dynamics stage and cleared. Neuron state (membrane potential, refractory counter, per-receptor currents, and any adaptation variables) lives in a per-worker neuron-state memory. Spikes emitted on firing are re-encoded to the global presynaptic identifier, merged by a round-robin arbiter, and returned to the APEIRON fabric, where they are routed to the cores hosting their postsynaptic targets, closing the loop.

The data plane is  $P$  words wide, where  $P$  is a configurable number of parallel synaptic-memory read lanes, and stages communicate through valid/ready handshakes with per-neuron buffering, so that the serial read-out of accumulated input overlaps the workers’ independent neuron updates. This delivery path scales with the number of workers but concentrates two costs that the prototype’s measurements reveal (Section 6): the synaptic-memory fetch, which dominates for densely-connected layers because every incoming spike retrieves its target population’s entire fanout, and the per-worker routing and round-robin merge, whose serialization grows with the spike load per timestep. Section 7 describes a redesign of this stage, a banked synaptic accumulator with independent read-modify-write lanes, that targets both.

### 3.3 Neuron model and numeric format

The neuron dynamics are a replaceable HLS kernel: leaky integrate-and-fire, integrate-and-fire, and adaptive-exponential models are currently sup-

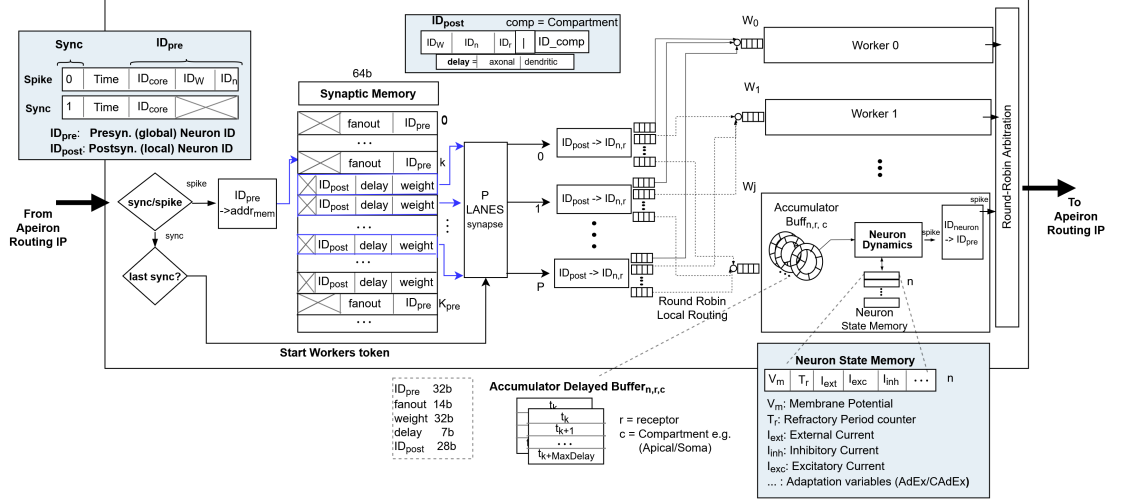


Figure 2: Prototype SNN core with local per-worker synaptic routing. Events arrive from the APEIRON communication IP carrying a leading sync bit: a spike event carries the presynaptic identifier ( $ID_{pre} = \langle ID_{core}, ID_W, ID_n \rangle$ ), a sync event only the originating core and timestep. A spike indexes the synaptic memory; the fetched fanout (weight, delay, receptor, destination  $ID_{post}$ ) is distributed to the destination workers, resolved to local (neuron, receptor) pairs, buffered in per-receptor FIFOs, and merged by a round-robin stage. Each worker accumulates contributions into per-(neuron, receptor) circular delay buffers ( $Buffer_{n,r}$ ), updates its neurons against the neuron-state memory, and emits spikes that are re-encoded and arbitrated back onto the fabric.

ported. The numeric representation is independently selectable between floating point and fixed point with tunable field widths, exposing the accuracy-versus-area/timing trade-off without touching the surrounding datapath.

## 4 Configuration and Generation Flow

An AIGOR instance is produced by an automated generation flow driven from a single declarative specification, rather than hand-specialized per network (Fig. 3). All structural choices, network topology, neuron model, numeric format, the degree of spatial versus temporal parallelism, and the partitioning of neurons across cores and workers, are captured in one YAML specification. A configuration stage expands it into the three artifacts that constitute an instance: the register-transfer description of the compute cores and their interconnect, the HLS neuron kernels, and the initialized synaptic-memory images that encode the target network’s connectivity. Because every

artifact is emitted from the same specification, an architectural variant is a one-line change rather than a manual rewiring across heterogeneous source files, which keeps systematic, reproducible exploration practical.

The processing cores, the workers, handlers, and the control and routing that ties them together, are authored as a parameterized cycle-accurate SystemC model and lowered to synthesizable RTL by Catapult HLS. The boundary and communication kernels (the I/O cores) are written as Vitis HLS tasks against the APEIRON API, and the most latency-sensitive synaptic datapath, the memory handler, is implemented in VHDL. These three paradigms are unified by the shared specification and build system, which emits the SystemC parameters, the VHDL configuration package, and the HLS task wiring.

The same SystemC description doubles as a fast functional simulator. It provides pre-synthesis validation of a configured instance, checking its numerical behavior and exercising the spike/sync protocol without committing to a full hardware build, and a complementary transaction-level (TLM) model of the routing IP lets multi-node topologies be simulated well beyond the available FPGA count; in this way the multi-node communication IP and the barrier-based timestep synchronization were exercised up to 1000 cores on a  $10 \times 10 \times 10$  torus, confirming the synchronization scheme at a scale beyond the available hardware. Networks enter the flow through a common ingestion path: recurrent models built in NEST [11] and feedforward models trained in snnTorch [10] are exported to a common intermediate representation, from which the toolchain derives the per-core synaptic-memory images. A single platform thus serves both the machine-learning-oriented and the neuroscience-oriented workloads usually addressed by separate tools.

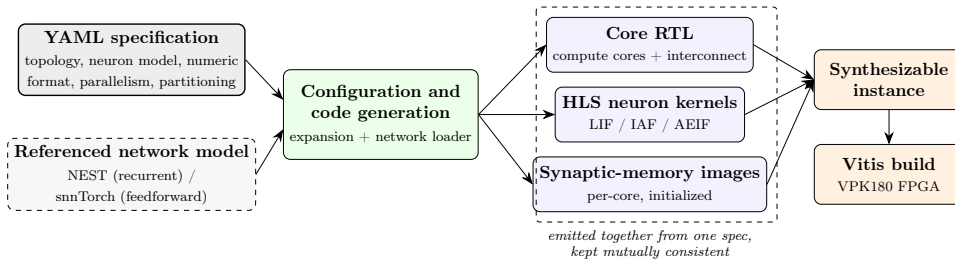


Figure 3: AIGOR configuration-driven generation flow. A single YAML specification is expanded by the code-generation stage into the core RTL, the HLS neuron kernels, and the initialized synaptic-memory images, which together form a synthesizable instance for the target FPGA platform.

## 5 Methodology and Benchmarks

We evaluate AIGOR with two contrasting workloads and characterize the configured instances for functional correctness and resource utilization. All hardware results are obtained on AMD Versal VPK180 devices (one or two boards depending on the benchmark). Unless otherwise stated, the datapath uses 32-bit fixed-point arithmetic with 12 integer bits.

### 5.1 Benchmarks

Both workloads use a leaky integrate-and-fire neuron, but each matches the conventions of its reference tool: the feedforward classifier follows the `snnTorch` `Leaky` neuron, the recurrent network the NEST `iaf_psc_delta` model. The two agree in their integration core and differ in minor details of reset and input handling, which the corresponding kernel configuration reproduces.

**Feedforward: spiking MNIST.** A fully-connected spiking classifier trained in `snnTorch` [10],  $256 \rightarrow 128 \rightarrow 10$  leaky integrate-and-fire neurons, with  $28 \times 28$  MNIST images downsampled on-chip to  $16 \times 16$  by the input core and rate-encoded over a 25-timestep window. Both layers are placed on a single core in the spatial (worker-parallel) organization of Section 3.2, where each neuron has its own datapath and the timestep dynamics of all the core’s neurons are computed in parallel (8 workers, 32 neurons each).

**Recurrent: balanced random network.** A Brunel-style [13] sparsely-connected excitatory/inhibitory network modeled in NEST [11] ( $\sim 1638$  excitatory / 410 inhibitory neurons, connection probability 0.1, driven by an 800 Hz Poisson source). This workload runs across multiple cores on two FPGAs and validates AIGOR on cyclic connectivity. Both networks are exported to the common intermediate representation and mapped onto the same architecture, differing only in configuration.

### 5.2 Functional validation and precision

For each benchmark we establish correctness against the software reference by deploying the configured instance on the FPGA and comparing its output under stimuli identical to the reference. The recurrent network is compared to its NEST reference at the spike level (matching spike times, or agreement of population statistics where fixed-point rounding accumulates); the classifier is compared to its `snnTorch` reference by classification accuracy. The same cycle-accurate SystemC model used during development provides an intermediate, pre-synthesis check. We assess the effect of fixed-point precision by comparing the hardware spike output against the reference at a

representative fixed-point setting and establishing the regime over which the two agree exactly; a full sweep across field widths is part of the planned characterization of Section 7.

## 6 Results

We report a first characterization of the prototype: functional validation on both workload classes, resource utilization on the VPK180, and validation of the multi-node synchronization scheme in simulation. The measured throughput of the prototype localizes the bottleneck that motivates the refinements of Section 7.

### 6.1 Functional correctness

On the feedforward benchmark, the deployed classifier reproduces the classification accuracy of its `snnTorch` reference ( $\sim 95\%$  on the MNIST test set) at the 25-timestep encoding window. On the recurrent benchmark, the FPGA reproduces the firing pattern of the NEST reference over the exercised interval (up to 3 ms of simulated time at a 0.1 ms timestep), on up to 4 cores on a single FPGA and up to 8 cores across two FPGAs. Under the representative fixed-point setting (32 total bits, 12 integer), the hardware reproduces the reference spike times *exactly* for up to  $\sim 2$  ms of simulated time 4; beyond that, fixed-point rounding gradually accumulates.

### 6.2 Throughput

On the classifier, over 10,000 MNIST samples, the single-core instance sustains 568 samples/s, measured with an on-chip cycle counter. Throughput is set by the spike load per timestep, and hence by the input encoding and connection density: for a fully-connected network at this scale the synaptic-memory fetch dominates, since each incoming spike retrieves its target population’s entire fanout. This is the primary bottleneck that the banked accumulator of Section 7 is designed to relieve.

### 6.3 Resource utilization

Table 2 reports post-implementation utilization on the VPK180 for a single core with the time-multiplexed worker, swept across workers ( $W$ ) and neurons per worker ( $n$ ). Utilization is LUT-dominated and scales with the degree of spatial parallelism; at 2048 neurons a single core uses of order one fifth of the device LUTs and a small fraction of its BRAM, with the synaptic image held on-chip. Scaling a single core beyond this was limited by place-and-route rather than by logic or memory capacity.

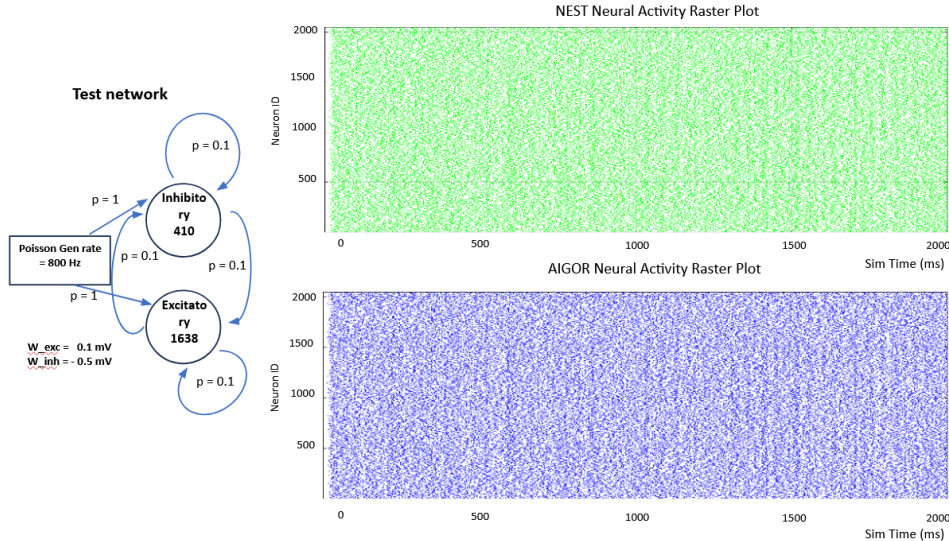


Figure 4: Functional validation on the recurrent benchmark. *Left*: the balanced random test network, a Brunel-style excitatory/inhibitory population of 1638 excitatory and 410 inhibitory leaky integrate-and-fire neurons with recurrent connection probability  $p = 0.1$  and synaptic weights  $W_{\text{exc}} = 0.1$  mV,  $W_{\text{inh}} = -0.5$  mV, driven by an 800 Hz Poisson source connected with  $p = 1$ . *Right*: spike raster of all 2048 neurons over the simulated interval (0.1 ms timestep) for the NEST reference (top) and the AIGOR FPGA instance (bottom). Both settle into the same asynchronous-irregular regime, and their population firing statistics agree across the window; exact per-spike agreement holds over the initial timesteps before fixed-point rounding diverges the individual neuron trajectories.

Table 2: Post-implementation utilization on the VPK180 (Total PL memory 994 Mb) for a single core with the time-multiplexed worker, as a function of workers ( $W$ ) and neurons per worker ( $n$ ).

Config ( $W \times n$ )	LUT	FF	DSP	BRAM	Syn. mem
16 n ( $4 \times 4$ )	0.40%	0.32%	0	0.04%	16 Kb
64 n ( $4 \times 16$ )	0.63%	0.47%	0	0.08%	197 Kb
512 n ( $4 \times 128$ )	2.25%	0.45%	0	0.32%	4 Mb
2048 n ( $32 \times 64$ )	22.7%	2.93%	2	1.94%	84 Mb
2048 n ( $16 \times 128$ )	21.1%	1.59%	34	1.30%	84 Mb

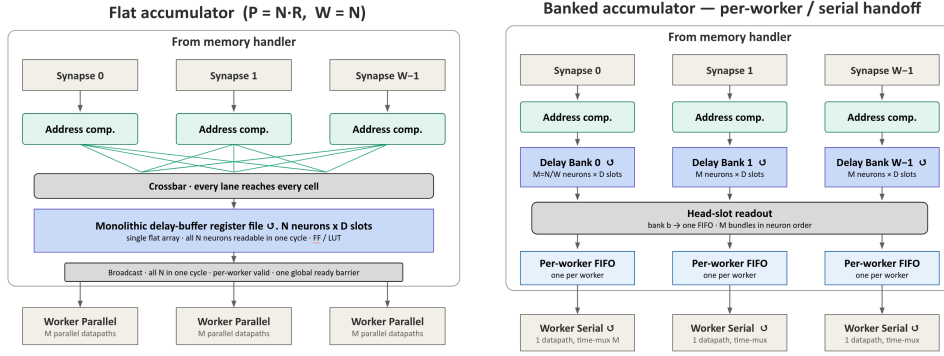
The worker-parallel organization trades on-chip memory for latency and throughput, and its two memories scale differently. The neuron-state memory grows linearly with the neuron count: in the spatial organization every neuron datapath must read and write its own state in the same cycle, so each neuron’s state occupies an independent memory block, and a single core of  $\sim 2\text{k}$  such neurons uses of order 33% of the device BRAM on state alone. Because a BRAM block exposes two ports, one block can back two neurons before a third would contend; time-multiplexing a group of neurons onto one datapath removes the per-neuron block at the cost of serialized updates, and is the lever used to place larger populations on a fixed budget. The synaptic memory, by contrast, grows with the connection count: for a fully-connected layer it scales quadratically with the neuron count, so the same  $\sim 2\text{k}$ -neuron core carries  $\sim 4\text{M}$  synapses. Held in URAM this reaches  $\sim 38\%$  of the device for this configuration and stays on-chip; beyond the on-chip capacity the synaptic image would have to move to off-chip DRAM, whose higher and less predictable access latency is especially costly for sparse SNNs, where the fanout reads are short and irregular rather than long bursts.

## 7 Architectural Refinements and Future Work

The prototype’s measured throughput points to two limits of the current core: the synaptic-delivery datapath and the global timestep barrier. This section sets out the refinements that address them. Each is an incremental addition to the same core rather than a new design, specified here ahead of implementation and on-FPGA measurement, together with the characterization we plan to run on the resulting instances.

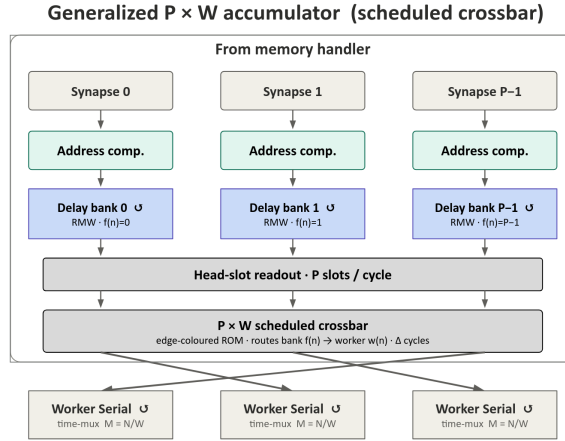
### 7.1 Banked synaptic accumulator

The prototype’s per-worker routing and round-robin merge (Section 3.2) serialize with the spike load. The proposed replacement moves accumulation into a shared bank of read-modify-write lanes: the neurons of a core are split into  $P$  banks updated in parallel by  $P$  lanes, one lane per bank, with no input crossbar or arbitration on the delivery path. The loader pre-sorts each presynaptic source’s fanout into  $P$  per-bank buckets, padded to a common length so the lanes advance together; the padding is small for the connectivity of interest, since a fully-connected layer splits evenly across banks and sparse random connectivity is balanced in expectation. Within a bank, each neuron’s pending input occupies a circular delay buffer addressed as  $\text{cell} \cdot \text{MAX\_DELAY} + ((\text{head} + \delta) \bmod \text{MAX\_DELAY})$ , with a write-first read and a sticky bypass register keeping repeated accumulation into the same cell coherent. Figure 5 lays out the design space this admits, from a fully-parallel flat point, through a per-worker banked point ( $P = W$ , banks aligned to workers), to a generalized  $P \times W$  point with a scheduled crossbar.



(a) Flat accumulator: fully parallel, single delay buffer, global synchronization.

(b) Banked accumulator: per-worker banking with streaming readout and time-multiplexed execution.



(c) Generalized  $P \times W$  banked accumulator with scheduled crossbar.

Figure 5: Design space for the banked synaptic-accumulator redesign. *Flat accumulator* (fully parallel): a crossbar matches every input lane to every cell of a single flat register-file delay buffer, which is read in one cycle and broadcast to all workers behind one global ready barrier; each worker steps its  $M$  neuron datapaths together. *Banked accumulator*, per-worker / serial handoff ( $P = W$ ,  $f$  aligned to  $w$ ):  $P$  addressable-RAM banks perform read-modify-write accumulation; the readout streams bank  $b$ 's  $M$  cells in order into one per-worker FIFO, and worker  $b$  time-multiplexes its  $M = N/W$  neurons over  $M$  cycles, rate-matched to the readout. *Generalized  $P \times W$  accumulator* (scheduled-crossbar handoff):  $f(n)$  maps a neuron to its bank,  $w(n)$  to its worker, with  $f(n) \neq w(n)$  in general; writes are bucketed by  $f(n)$  (no input crossbar) with compile-time pre-resolved bank-local addresses, and at the barrier a  $P \times W$  crossbar, configured per cycle by a compile-time edge-colouring, routes each bank's head-slot stream to worker  $w(n)$  in  $\Delta$  cycles (crossing lines show one edge-colour). Throughout, a cell is one neuron's circular delay line within its bank, one MAX\_DELAY-slot buffer holding  $R$  receptor accumulators per slot.

## 7.2 Inter-core routing topology

The refined communication IP also makes the way cores address one another over the routing IP configurable, following the connectivity of the mapped network (Fig. 6). In *feedforward* operation each core sends its output spikes only to the cores that host postsynaptic targets, using per-core routing tables resolved at generation time; delivery is directed (point-to-point) over the switch, and the receiving core’s presynaptic address space stays compressed to its few upstream sources, keeping the occupied synaptic memory small. Directed delivery combined with a layer-per-core mapping also relieves the input port: a core in a feedforward pipeline ingests only the spikes of its single upstream layer, rather than contending for the same port between an upstream source and its own re-injected output as a broadcasting core does, so per-core input bandwidth translates more directly into throughput. In *recurrent* operation each core broadcasts its output over the switch to all cores, the general case for arbitrary cyclic connectivity, and the presynaptic address space expands to the global source set. The two modes share the same cores and the same switch; only the addressing policy and the resulting per-core memory sizing differ.

For the networks recurrent operation targets, broadcast is less wasteful than it appears. In a sparsely-connected balanced network distributed across a modest number of cores, a neuron’s spike is likely to have at least one postsynaptic target on most cores, so directed delivery would in any case replicate the spike widely; at the scales considered here broadcast and directed delivery converge, while broadcast avoids per-source routing state.

## 7.3 Fused single-word spike/sync protocol

The prototype spends a dedicated packet on the per-timestep barrier (Section 3.1). Moving the communication IP from a payload-carrying format to a header-only, single-word format lets the end-of-timestep marker ride on the last spike-carrying word, removing the dedicated synchronization transaction; the gain is largest for throughput-bound feedforward inference, where synchronization would otherwise be a fixed per-timestep tax.

## 7.4 Neighbor-local synchronization and stochastic input

The current global barrier, in which every core exchanges a sync with every other, scales poorly with core count. Restricting synchronization to nearest neighbors on the torus, a globally-asynchronous locally-synchronous (GALS) scheme, removes the all-to-all exchange while preserving per-timestep spike ordering. Independently, a Poisson spike generator embedded in each worker can supply the background stochastic activity that bio-inspired networks require, without carrying it over the fabric.

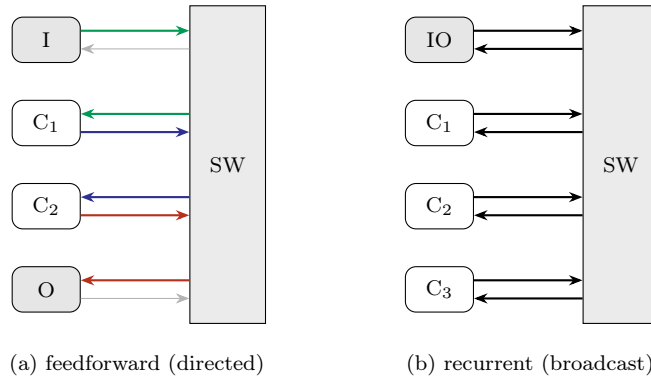


Figure 6: The two configurable routing modes over the APEIRON switch, introduced by the refined communication IP. Every core port is bidirectional (two arrows per link). (a) Feedforward: the input core injects to  $C_1$  (green leg,  $I \rightarrow SW \rightarrow C_1$ ), which routes via the switch through  $C_2$  before forwarding to the output core (red legs); unused legs are greyed. Delivery is directed and point-to-point, though it still traverses the switch. (b) Recurrent: a single I/O core and the compute cores all exchange over the switch, and each core’s output is broadcast to all cores, supporting arbitrary cyclic connectivity. The same cores and switch serve both modes; only the addressing policy changes.

## 7.5 Design-space characterization

Once these refinements are in place, the more interesting object of study is the design space itself, which the configuration axes make directly measurable. The same network can be regenerated across the numeric-format, folding, banking-degree ( $P$ ), and worker-count axes, and each resulting instance placed and measured on the same device, turning qualitative architectural trade-offs into a Pareto surface of accuracy against area, latency, and energy. A full fixed-point field-width sweep maps the accuracy-versus-cost front of a single workload; sweeping the folding and banking axes at fixed accuracy maps the latency-versus-area front; and running the same two workload classes through the identical flow lets the feedforward and recurrent operating points be compared on one substrate rather than across separate systems.

Energy anchors this surface. From switching activity, representative stimulus is simulated to produce a switching-activity record (SAIF) that drives the vendor power-analysis tool to yield average power for a configured instance; energy per inference (feedforward) or per simulated biological second (recurrent) then follows from the measured runtime. Reported in neuromorphic conventions, energy per synaptic operation (pJ/SOP) and energy per inference ( $\mu\text{J}/\text{inference}$ ), these figures are read as relative comparisons across AIGOR configurations, letting the design space be ranked by effi-

ciency rather than compared as absolute claims against ASIC neuromorphic processors.

## 8 Conclusion

We have presented AIGOR, a modular, event-driven neuromorphic architecture for configurable SNN inference. AIGOR treats the neuron model, numeric precision, and the mapping of neurons onto workers and cores as configuration axes of one architecture rather than as design-time commitments, and it derives a complete synthesizable instance, cores, neuron kernels, and initialized synaptic-memory images, from a single declarative specification. A first prototype on the Versal VPK180 runs two workloads usually handled by separate systems, a feedforward `snnTorch` classifier and a recurrent NEST balanced random network, on the same cores: the classifier reproduces its reference accuracy, and the recurrent network matches its NEST reference at the spike level across cores spanning two FPGAs. We characterized the prototype's resource utilization and validated the multi-node synchronization scheme in simulation up to one thousand cores. The measured throughput localizes the bottleneck in the synaptic-delivery datapath and the global barrier, and motivates a banked synaptic accumulator, a fused spike/sync protocol, and neighbor-local synchronization, now in development, each expressible as a change to the same configurable cores. The architecture's parameterized structure makes it a natural platform for the systematic exploration of SNN hardware design trade-offs.

## Acknowledgments

P. Perticaroli is a PhD student enrolled in the National PhD program in Artificial Intelligence, XXXIX cycle, course on Health and Life Sciences, organized by Università Campus Bio-Medico di Roma.

## References

- [1] K. Boahen, *Point-to-point connectivity between neuromorphic chips using address events*, IEEE Trans. Circuits Syst. II 47 (2000) 416, doi:10.1109/82.842110.
- [2] R. Ammendola et al., *APEIRON: a Framework for High Level Programming of Dataflow Applications on Multi-FPGA Systems*, EPJ Web Conf. 295 (2024) 11002 (CHEP 2023), doi:10.1051/epjconf/202429511002.
- [3] J. Duarte et al., *Fast inference of deep neural networks in FPGAs for particle physics*, JINST 13 (2018) P07027.

- [4] T. Aarrestad et al., *Fast convolutional neural networks on FPGAs with hls4ml*, Mach. Learn.: Sci. Technol. 2 (2021) 045015.
- [5] P. Perticaroli et al., *Achieving Low-Latency, High-Throughput On-line Partial Particle Identification for the NA62 Experiment Using FPGAs and Machine Learning*, Electronics 14 (2025) 1892, doi:10.3390/electronics14091892.
- [6] J. Anderson et al., *FELIX: a high-throughput network approach for interfacing to front-end electronics for ATLAS experiments*, J. Phys.: Conf. Ser. 664 (2015) 082050.
- [7] S. Vallarino et al., *The dual-radiator RICH detector of the ePIC experiment at the EIC*, Nucl. Instr. Meth. A (2024) 168834.
- [8] W. Maass, *Networks of spiking neurons: The third generation of neural network models*, Neural Networks 10 (1997) 1659.
- [9] W. Gerstner, W.M. Kistler, R. Naud, L. Paninski, *Neuronal Dynamics: From Single Neurons to Networks and Models of Cognition*, Cambridge University Press, 2014.
- [10] J.K. Eshraghian, M. Ward, E.O. Neftci, X. Wang, G. Lenz, G. Dwivedi, M. Bennamoun, D.S. Jeong, W.D. Lu, *Training Spiking Neural Networks Using Lessons From Deep Learning*, Proc. IEEE 111 (2023) 1016, doi:10.1109/JPROC.2023.3308088.
- [11] M.-O. Gewaltig, M. Diesmann, *NEST (NEural Simulation Tool)*, Scholarpedia 2 (2007) 1430.
- [12] B. Golosio, G. Tiddia, C. De Luca, E. Pastorelli, F. Simula, P.S. Paolucci, *Fast Simulations of Highly-Connected Spiking Cortical Models Using GPUs*, Front. Comput. Neurosci. 15 (2021) 627620, doi:10.3389/fncom.2021.627620.
- [13] N. Brunel, *Dynamics of sparsely connected networks of excitatory and inhibitory spiking neurons*, J. Comput. Neurosci. 8 (2000) 183.
- [14] K. Roy, A. Jaiswal, P. Panda, *Towards spike-based machine intelligence with neuromorphic computing*, Nature 575 (2019) 607.
- [15] C.D. Schuman, S.R. Kulkarni, M. Parsa, J.P. Mitchell, P. Date, B. Kay, *Opportunities for neuromorphic computing algorithms and applications*, Nat. Comput. Sci. 2 (2022) 10.
- [16] M. Davies et al., *Loihi: A neuromorphic manycore processor with on-chip learning*, IEEE Micro 38 (2018) 82.

- [17] G. Orchard et al., *Efficient Neuromorphic Signal Processing with Loihi 2*, in 2021 IEEE Workshop on Signal Processing Systems (SiPS), 2021, p. 254.
- [18] P.A. Merolla et al., *A million spiking-neuron integrated circuit with a scalable communication network and interface*, Science 345 (2014) 668.
- [19] J. Pei et al., *Towards artificial general intelligence with hybrid Tianjic chip architecture*, Nature 572 (2019) 106.
- [20] J. Schemmel, D. Brüderle, A. Grübl, M. Hock, K. Meier, S. Millner, *A wafer-scale neuromorphic hardware system for large-scale neural modeling*, in Proc. IEEE ISCAS, 2010, p. 1947.
- [21] S.B. Furber, F. Galluppi, S. Temple, L.A. Plana, *The SpiNNaker Project*, Proc. IEEE 102 (2014) 652.
- [22] C. Mayr, S. Höppner, S. Furber, *SpiNNaker 2: A 10 Million Core Processor System for Brain Simulation and Machine Learning*, arXiv:1911.02385 (2019).
- [23] S. Deng, D. Yu, C. Lv, X. Du, L. Jiang, X. Zhao, W. Tong, X. Zheng, W. Fang, P. Zhao, G. Pan, S. Dustdar, A.Y. Zomaya, *Edge Intelligence with Spiking Neural Networks*, arXiv:2507.14069 (2025).
- [24] E.O. Neftci, H. Mostafa, F. Zenke, *Surrogate Gradient Learning in Spiking Neural Networks*, IEEE Signal Processing Magazine 36 (2019) 51.
- [25] S.R. Kulkarni et al., *On-Sensor Data Filtering using Neuromorphic Computing for High Energy Physics Experiments*, in Proceedings of the 2023 International Conference on Neuromorphic Systems (ICONS '23), doi:10.1145/3589737.3605976.
- [26] E. Coradin et al., *Unsupervised Particle Tracking with Neuromorphic Computing*, arXiv:2307.11242.
- [27] K. Kauth, T. Stadtmann, V. Sobhani, T. Gemmeke, *neuroAIx: A high-performance, energy-efficient and reconfigurable accelerator for neuroscientific spiking neural networks*, Front. Comput. Neurosci. 17 (2023) 1144143.
- [28] A. Carpegna, A. Savino, S. Di Carlo, *Spiker+: A Framework for the Generation of Efficient Spiking Neural Networks FPGA Accelerators for Inference at the Edge*, IEEE Trans. Emerg. Topics Comput. (2024), doi:10.1109/TETC.2024.3511676.
- [29] M. Farahani, M.R. Roshanshah, S. Safari, *Flexi-NeurA: A Configurable Neuromorphic Accelerator with Adaptive Bit-Precision Exploration for Edge SNNs*, arXiv:2602.18140 (2026).

- [30] M.I. Al Hafiz, A. Podobas, *NeuroRing: Scaling Spiking Neural Networks via Multi-FPGA Bidirectional Ring Topologies and Stream-Dataflow Architectures*, arXiv:2604.28059 (2026).
- [31] A. Gautam, P. Date, S. Kulkarni, R. Patton, T. Potok, *NeuroCoreX: An Open-Source FPGA-Based Spiking Neural Network Emulator with On-Chip Learning*, arXiv:2506.14138 (2025).
- [32] P. Perticaroli et al., *AIGOR for online data reduction at the ePIC dRICH*, in preparation (2026).